ARTICLE

Simulation of the Hydraulic Behavior of a Bionic-Structure Drip Irrigation Emitter

Tianyu Xu[1], Yanru Su[1], Zhouming Su[1], Shuteng Zhi[1], Ennan Zheng[1,*] and Chengcheng Yan[2]

[1]School of Hydraulic and Electric Power, Heilongjiang University, Harbin, 150080, China

[2]School of Traditional Chinese Medicine, Zhejiang Pharmaceutical College, Ningbo, 315503, China

[*]Corresponding Author: Ennan Zheng. Email: xty1115291208@163.com

ABSTRACT

The bionic structure drip irrigation emitter (BSDE) is a new-type emitter, by which better hydraulic performances can be obtained. In the present work, twenty-five sets of orthogonal test schemes were implemented to analyze the influence of the geometric parameters of the flow channel on the hydraulic characteristics and energy dissipation efficiency of this emitter. Through numerical simulations and verification tests, the flow index and energy dissipation coefficient were obtained. According to the results, the flow index of the BSDE is 0.4757–0.5067. The energy dissipation coefficient under the pressure head of 5–15 m is 584–1701. The verification test has shown that the relative errors among measured values, simulated values and estimated values are less than 3%, which indicates that the flow index can be estimated reliably.

KEYWORDS

BSDE; flow index; energy dissipation; numerical simulation; verification test

1 Introduction

Drip irrigation emitter is the core component of the drip irrigation system. The flow channel of the drip irrigation emitter affects the hydraulic performance and energy dissipation efficiency [1,2]. The hydraulic performance of the flow channel is expressed by the flow index, which indicates the sensitivity of the flow rate of the drip irrigation emitter to the inlet pressure [3,4]. The energy dissipation efficiency of the flow channel is expressed by the energy dissipation coefficient, which indicates the intensity of flow turbulence in drip irrigation emitter [5]. The geometric parameters of the flow channel have a significant impact on the uniformity and efficiency of the drip irrigation system [6,7]. Excessive geometric parameters will cause the uniformity of irrigation to decrease, and small geometric parameters will reduce the energy dissipation efficiency [8,9]. Therefore, the research on the relationship between the geometric parameters and the hydraulic performance of flow channels has always been a hot topic in the field of water-saving irrigation [10,11].

Computational fluid dynamics (CFD) is a new method to study the flow mechanism of emitters, reduce the development cost of emitters and shorten the test period, which makes up for the deficiency of the experiment to a certain extent [12,13]. Yuan et al. [14] used the CFD method to optimize the structure of the divided-flow drip irrigation emitter to obtain the functional relationship between anti-blocking performance and geometric parameters. Guo et al. [15] designed a two-way opposed flow channel and

applied CFD to analyze the relationship between flow rate and working pressure. In order to improve the hydraulic performance and energy dissipation efficiency, many scholars had put forward many new design concepts and structural types of drip irrigation emitters [16,17]. The fractal flow channel designed on the basis of fractal theory can effectively reduce the flow index [18]. The triangle circulation flow channel can increase fluid turbulence and improve the uniformity of outlet flow-through internal large and small triangles [19]. A two-way flow channel with the combination of "V" shape and "∧" shape can improve the energy dissipation efficiency by mixing forward and reverse flow [20]. Xing et al. [21] used the bionic principle to design the drip irrigation emitter with a perforated plate structure, which had good hydraulic performance, and the flow index was 0.47–0.51.

Many inventions were derived from the bionics of plant structure or form, and plant bionics had a very wide range of applications. Based on the pressure drop similarity between the drip irrigation emitter and the torus-margo bordered pit structure of the plant xylem, the pit drip irrigation emitter was designed [22,23]. The bionic structure drip irrigation emitter (BSDE) was taken as the research objectives, numerical simulation and tests used to obtain pressure, and flow rate in the flow channel, combined with multiple regression models to establish a mathematical equation for calculating the flow index. It can: (1) obtain the flow index and the energy dissipation coefficient of the BSDE, (2) analyze the influence of geometric parameters on the performance of the BSDE, (3) evaluate the prediction model and flow characteristics of the BSDE. The results will provide a reference for the new bionic structure drip irrigation emitters and offer a deeper understanding of channel design in the drip irrigation technology.

2 Materials and Methods

2.1 BSDE Structure Design

The torus-margo bordered pit structure in plant xylem tracheids had good depressurization stability (Fig. 1a). According to the structure similarity, the pit drip irrigation emitter (PDIE) was designed [23]. Later research found that the BSDE had better working performance than the PDIE. The structure of PDIE and BSDE were shown in Figs. 1b and 1c.

(a) pit structure   (b) PDIE   (c) BSDE
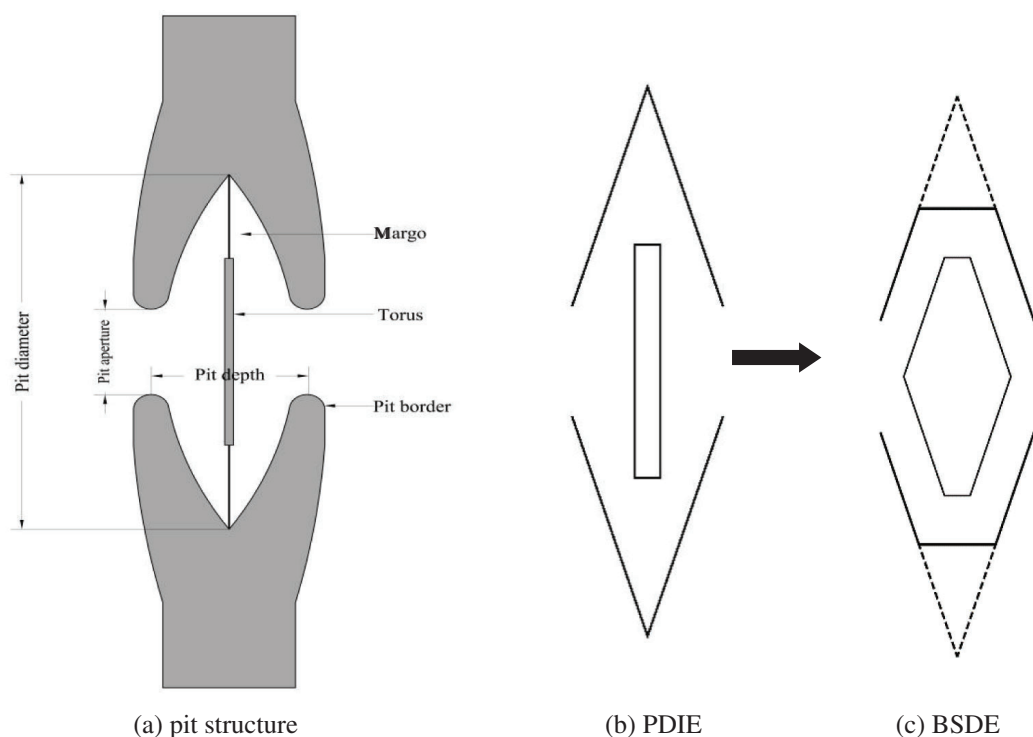
Figure 1: Schematic diagram of pit structure and two bionic models

2.2 Numerical Simulation and Test Model

2.2.1 Control Equation

The fluid flow relies on the steady-state conservation equations for mass and momentum in a fluid, which are given by [24,25]:

Continuity equation:

$$\frac{\partial u}{\partial x} + \frac{\partial v}{\partial y} + \frac{\partial w}{\partial z} = 0 \tag{1}$$

Momentum equation:

$$\begin{cases} \rho\left(u\frac{\partial u}{\partial x} + v\frac{\partial u}{\partial y} + w\frac{\partial u}{\partial z}\right) = -\frac{\partial P}{\partial x} + \mu\left(\frac{\partial^2 u}{\partial x^2} + u\frac{\partial^2 u}{\partial y^2} + u\frac{\partial^2 u}{\partial z^2}\right) \\ \rho\left(u\frac{\partial v}{\partial x} + v\frac{\partial v}{\partial y} + w\frac{\partial v}{\partial z}\right) = -\frac{\partial P}{\partial y} + \mu\left(\frac{\partial^2 v}{\partial x^2} + u\frac{\partial^2 v}{\partial y^2} + u\frac{\partial^2 v}{\partial z^2}\right) \\ \rho\left(u\frac{\partial w}{\partial x} + v\frac{\partial w}{\partial y} + w\frac{\partial w}{\partial z}\right) = -\frac{\partial P}{\partial z} + \mu\left(\frac{\partial^2 w}{\partial x^2} + u\frac{\partial^2 w}{\partial y^2} + u\frac{\partial^2 w}{\partial z^2}\right) \end{cases} \tag{2}$$

where u, v, w are the components of the velocity vector along the x, y, z-directions, respectively, ρ is the fluid density, P is the fluid pressure, μ is the dynamic viscosity.

In this study, a non-direct numerical simulation method was selected for analysis. The standard k–ε model had strong applicability to turbulent flow involved in BSDE model.

Its control equations are as follows:

$$\frac{\partial(\rho K)}{\partial t} + \frac{\partial(\rho k u_i)}{\partial x_i} = \frac{\partial}{\partial x_i}\left[\left(\mu + \frac{\mu_t}{\sigma_k}\right)\frac{\partial k}{\partial x_j}\right] + G_k + G_b - \rho\varepsilon - Y_M + S_k$$

$$\frac{\partial(\rho\varepsilon)}{\partial t} + \frac{\partial(\rho\varepsilon u_i)}{\partial x_i} = \frac{\partial}{\partial x_j}\left[\left(\mu + \frac{\mu_t}{\sigma_\varepsilon}\right)\frac{\partial\varepsilon}{\partial x_j}\right] + C_{1\varepsilon}\frac{\varepsilon}{k}(G_k + C_{3\varepsilon}G_b) - C_{2\varepsilon}\rho\frac{\varepsilon^2}{k} + S_\varepsilon \tag{3}$$

In the model, ε representing the turbulent dissipation rate was defined as:

$$\varepsilon = \frac{\mu}{\rho}\overline{\left(\frac{\partial u'_i}{\partial x_k}\right)\left(\frac{\partial u'_j}{\partial x_k}\right)} \tag{4}$$

G_k representing the generation term of the turbulent energy k due to the average velocity gradient was defined as:

$$G_k = \mu_t\left(\frac{\partial u_i}{\partial x_j} + \frac{\partial u_j}{\partial x_i}\right)\frac{\partial u_i}{\partial x_j} \tag{5}$$

Turbulent viscosity μ_t can be expressed as a function of k and ε as follows:

$$\mu_t = \rho C_\mu\frac{k^2}{\varepsilon} \tag{6}$$

where G_b was the generic term of the kinetic energy k caused by buoyancy, Y_M represented the contribution of pulsation expansion in compressible turbulence, $C_{1\varepsilon}$, $C_{2\varepsilon}$ and $C_{3\varepsilon}$ were the empirical constant, σ_k and σ_ε were the Prandtl numbers corresponding to the kinetic energy k and the turbulent dissipation rate ε, respectively. C_μ was empirical constant, S_k and S_ε were user-defined source items, and the correlation values were: $C_{1\varepsilon} = 1.44$, $C_{2\varepsilon} = 1.92$, $C_{3\varepsilon} = 1.44$, $\sigma_k = 1.0$, $\sigma_\varepsilon = 1.3$, $G_b = 0$, $Y_M = 0$, $C_\mu = 0.09$, $S_k = 0$, $S_\varepsilon = 0$.

2.2.2 Structure and Geometric Parameters

The BSDE model was composed of inlet, flow channel and outlet (Fig. 2). The flow channel included pit aperture A(mm), pit depth B(mm), bottom height C(mm), left width E(mm) and right width D(mm) (Fig. 3a).
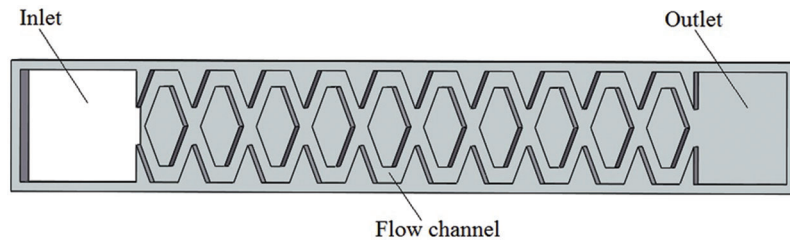
Figure 2: Schematic diagram of BSDE model

(a) Geometric parameters   (b) Fluid domain meshing
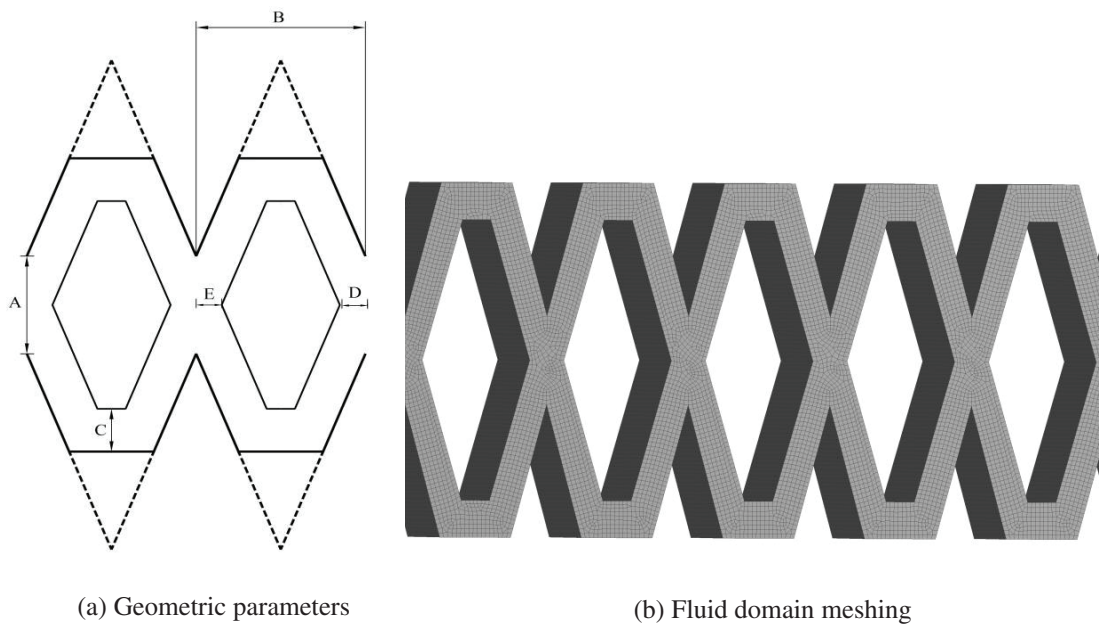
Figure 3: Schematic diagram of the geometric parameters and meshing

The value range of geometric parameters of the flow channel was as follows: A was 0.6 mm–1.0 mm, B was 1.0 mm–1.4 mm, C was 0.25 mm–0.45 mm, D was 0.12 mm–0.24 mm, E was 0.12 mm–0.24 mm. The pit diameter of the unit was 2.4 mm. The depth of BSDE model was 0.8 mm and the number of channel units was 10.

2.2.3 Meshing and Boundary Conditions

The BSDE model was built by SolidWorks software. The fluid domain was divided by unstructured grids of tetrahedron and hexahedron. Based on the prediction accuracy of the inlet and outlet pressure drop, the predicted pressure drop difference was less than 0.5% (Table 1), and it was considered that the number of grids had no effect on the numerical simulation results. The maximum element size was 3×10^{-5} m, the minimum element size was 1×10^{-5} m, and the total element number of the fluid domain was about 0.39 million. The grid of flow channels were shown in Fig. 3b.

Table 1: Grid independence test

	Number of grid	Pressure drop
Very Coarse	117450	–
Coarse	205634	1.27%
Standard	388276	0.58%
Fine	939874	0.21%

The spatial discretization was based on the finite volume method. The second-order upwind scheme was adopted for the convection term. The coupling of velocity and pressure was solved by the SIMPLE algorithm, and the accuracy control standard was set to 10^{-5}. The time step size was 0.02 s, Number of time step was 1000. The inlet of the flow channel was set to the pressure inlet, and the pressure values were set to 50, 75, 100, 125, 150, 175, 200, 225 and 250 kPa, respectively; the flow channel outlet was set to the outflow boundary. The no-slip condition was applied to the wall faces of the flow channel. The computing hardware platform was the five PowerCube-S01 cloud cubes high-performance parallel computers, and the ANSYS FLUENT 17.1 calculation software was used.

2.2.4 Construction of Test Model

The test rigs were 5 sets of test models. A pressure level set of tests was designed to each time 25 kPa increase within the pressure range of 50–250 kPa. Each test lasts 15 minutes, and 3 times of test measurements were done under each pressure level to take the average values. The BSDE models were made of plexiglass. An EM-G32S-X32 high-precision engraving machine with a manufacturing precision of 0.01 mm was used, and a repeating positioning accuracy was 0.005 mm. The physical picture of the plexiglass test model was shown in Fig. 4.
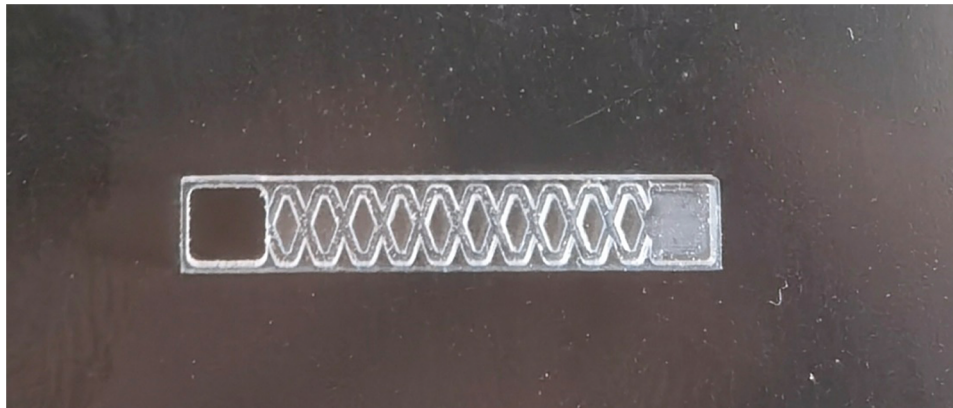
Figure 4: Prototype of BSDE model

2.3 Orthogonal Experiment Scheme

The geometric parameters of BSDE have adopted five factors and five levels (Table 2) and were designed according to the orthogonal experimental design table L25(5^6). The structure parameters values were shown in Table 3.

Table 2: Geometry parameters values of BSDE model

Level	Geometry parameters values				
	A/mm	B/mm	C/mm	D/mm	E/mm
1	0.6	1.0	0.25	0.12	0.12
2	0.7	1.1	0.30	0.15	0.15
3	0.8	1.2	0.35	0.18	0.18
4	0.9	1.3	0.40	0.21	0.21
5	1.0	1.4	0.45	0.24	0.24

Note: A is distance of pit aperture, mm; B is distance of pit depth, mm; C is distance of bottom height, mm; D is distance of right width, mm; E is distance of left width, mm.

Table 3: Orthogonal experiment scheme of BSDE model

| Level	Geometry parameters values				
	A/mm	B/mm	C/mm	D/mm	E/mm
1	0.6	1.0	0.25	0.12	0.12
2	0.6	1.1	0.30	0.15	0.15
3	0.6	1.2	0.35	0.18	0.18
4	0.6	1.3	0.40	0.21	0.21
5	0.6	1.4	0.45	0.24	0.24
6	0.7	1.0	0.30	0.18	0.21
7	0.7	1.1	0.35	0.21	0.24
8	0.7	1.2	0.40	0.24	0.12
9	0.7	1.3	0.45	0.12	0.15
10	0.7	1.4	0.25	0.15	0.18
11	0.8	1.0	0.35	0.24	0.15
12	0.8	1.1	0.40	0.12	0.18
13	0.8	1.2	0.45	0.15	0.21
14	0.8	1.3	0.25	0.18	0.24
15	0.8	1.4	0.30	0.21	0.12
16	0.9	1.0	0.40	0.15	0.24
17	0.9	1.1	0.45	0.18	0.12
18	0.9	1.2	0.25	0.21	0.15
19	0.9	1.3	0.30	0.24	0.18
20	0.9	1.4	0.35	0.12	0.21
21	1.0	1.0	0.45	0.21	0.18
22	1.0	1.1	0.25	0.24	0.21
23	1.0	1.2	0.30	0.12	0.24
24	1.0	1.3	0.35	0.15	0.12
25	1.0	1.4	0.40	0.18	0.15

2.4 Calculation Method of Energy Dissipation Efficiency, Flow Index and Relative Error

The model can analyze the fluid flow in BSDE (Fig. 5) by the energy conservation law (Bernoulli equation). The flow between arbitrary sections satisfies the Bernoulli equation, which was written in sections from the inlet to the exit sections Z_1, Z_2, Z_n as:

$$\frac{P_1}{\rho g} + \frac{V_1^2}{2g} + z_1 = \frac{P_2}{\rho g} + \frac{V_2^2}{2g} + z_2 + \xi_1 \frac{V_2^2}{2g} + \lambda \frac{l_1 V_2^2}{8Dg}$$

$$\frac{P_2}{\rho g} + \frac{V_2^2}{2g} + z_1 = \frac{P_3}{\rho g} + \frac{V_3^2}{2g} + z_3 + \xi_2 \frac{v_3^2}{2g} + \lambda \frac{l_2 V_3^2}{8Dg} \qquad (7)$$

$$......$$
$$......$$

$$\frac{P_{n-1}}{\rho g} + \frac{V_{n-1}^2}{2g} + z_{n-1} = \frac{P_n}{\rho g} + \frac{V_n^2}{2g} + z_n + \xi_{n-1} \frac{V_n^2}{2g} + \lambda \frac{l_{n-1} V_n^2}{8Dg}$$

where P_n and V_n were the average pressure and flow velocity at section n, ρ was fluid density, g was the acceleration of gravity, z_n was the position head of water at the section, ξ_{n-1} was the local loss coefficient of section $n-1$ to section n, λ was the friction factor of head loss, l_{n-1} was the length between two adjacent sections. D was the hydraulic radius of the rectangular section flow channel. And a and b were the width and depth of the flow channel section, the expression of D was:

$$D = \frac{A}{\chi} = \frac{ab}{2(a+b)} \qquad (8)$$
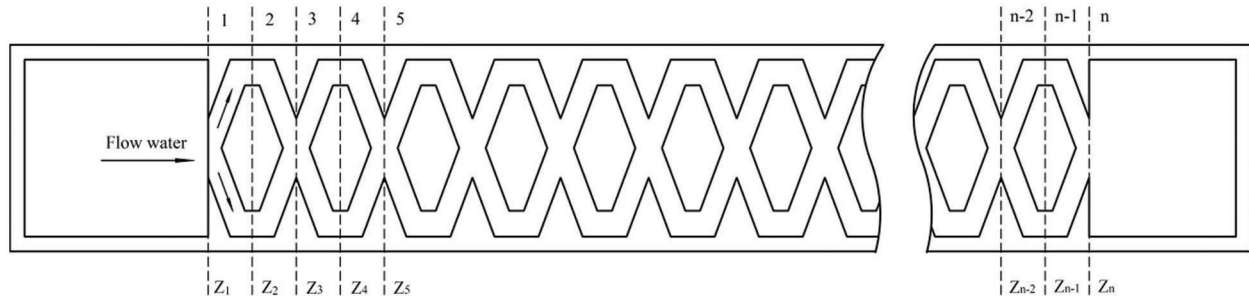
Figure 5: Schematic diagram of flow mechanism in BSDE model

Add the two sides of the equations of Eq. (7) in order:

$$\frac{P_1 - P_n}{\rho g} = z_n - z_1 + \xi_1 \frac{V_2^2}{2g} + \xi_2 \frac{V_3^2}{2g} + \cdots + \xi_{n-1} \frac{V_n^2}{2g} + \lambda \frac{L V_n^2}{8Dg} \qquad (9)$$

where $l_1 + l_2 + l_3 + \cdots + l_{n-1} = L$, L was the total length of the flow channel. Positioning head due to the horizontal flow path, so $Z_1 = Z_2 = Z_3 = \cdots = Z_n$.

Known by the continuity equation:

$$V_1 A_1 = V_2 A_2 = V_3 A_3 = \cdots = V_n A_n \qquad (10)$$

In Eq. (10), $A_i (i=1,2...,n)$ was the flow area at the corresponding section, substituting Eq. (10) into Eq. (9) give:

$$\frac{\Delta P}{\rho g} = \left[\lambda \left(\frac{A_1}{A_n} \right)^2 \frac{L}{4D} + \sum_{i=1}^{n-1} \xi_i \left(\frac{A_1}{A_{i+1}} \right)^2 \right] \frac{V_1^2}{2g} \tag{11}$$

where

$$\xi = \left[\lambda \left(\frac{A_1}{A_n} \right)^2 \frac{L}{4D} + \sum_{i=1}^{n-1} \left(\frac{A_1}{A_{i+1}} \right)^2 \xi_i \right] \tag{12}$$

Eq. (11) was simplified to:

$$\frac{\Delta P}{\rho g} = \xi \frac{V_1^2}{2g} \tag{13}$$

Expressed as:

$$\xi = \frac{2}{V_1^2} \cdot \frac{\Delta P}{\rho} \tag{14a}$$

Expressed by flow rate:

$$\xi = \frac{2a^2 b^2}{q^2} \cdot \frac{\Delta P}{\rho} \tag{14b}$$

In Eqs. (14a) and (14b), ξ was the flow channel energy dissipation coefficient (frictional head loss and local head loss), q was the average flow rate of the flow channel. Obviously, ξ reflected energy dissipation capacity of BSDE. The expression of q was:

$$q = kH^x \tag{15}$$

where k was the flow coefficient; H was the inlet pressure, kPa; x was the flow index.

The relative error equation was as follows:

$$\varepsilon = \frac{S(T) - E}{S(T)} \times 100\% \tag{16}$$

where ε was the relative error; S was the simulation value, l/h; T was the test value, l/h; and E was the estimated value, l/h.

3 Result

### 3.1 Flow-Pressure Relationship and Flow Index of Flow Channel

The orthogonal experiment numerical simulation results were shown in Table 4. Formula (15) was used to fit the relationship between flow rate and pressure, the coefficient of determination was 0.9998-0.9999, and the regression equation had a good correlation. The flow index of different geometric parameters was between 0.4757–0.5067. The schemes 12 and 18 were taken as examples (Fig. 6), the root means square error between the fitted value and the experiment value was 0.0053 and 0.0090 L/h, which more accurately reflected the relationship between the pressure and flow rate of the BSDE.

Table 4: Orthogonal experiment numerical simulation results

Level	Flow rate $q/\ \mathrm{L \cdot h^{-1}}$	Flow coefficient	Flow index	Level	Flow rate $q/\ \mathrm{L \cdot h^{-1}}$	Flow coefficient	Flow index
1	1.676	0.2339	0.5037	14	2.375	0.3480	0.4907
2	1.980	0.2748	0.5036	15	2.428	0.3555	0.4905
3	2.213	0.3187	0.4949	16	2.258	0.3203	0.4981
4	2.465	0.3559	0.4941	17	2.173	0.3345	0.4777
5	2.725	0.3918	0.4954	18	2.110	0.3270	0.4757
6	2.078	0.2854	0.5067	19	2.505	0.3804	0.4820
7	2.368	0.3350	0.4995	20	2.828	0.4039	0.4970
8	2.174	0.3337	0.4781	21	2.187	0.3318	0.4816
9	2.411	0.3481	0.4944	22	2.109	0.3071	0.4925
10	2.382	0.3356	0.5009	23	2.472	0.3630	0.4904
11	2.024	0.2955	0.4917	24	2.574	0.3785	0.4894
12	2.254	0.3228	0.4958	25	2.859	0.4274	0.4853
13	2.501	0.3746	0.4854				

Note: q, flow rate value under inlet pressure 50 kPa; Flow index was estimated by regression model.

(a) Experiment scheme 12   (b) Experiment scheme 18
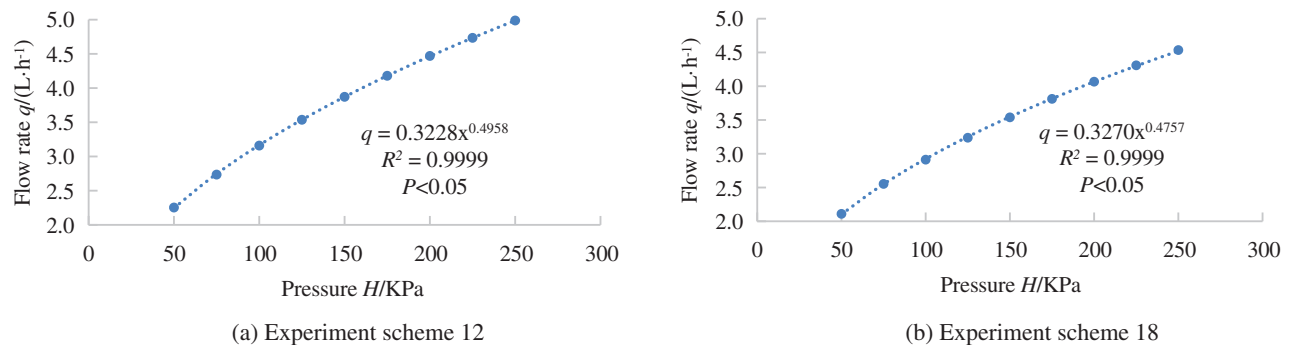
Figure 6: Relationship between flow rate and pressure for test schemes 12 and 18

3.2 Energy Dissipation Efficiency and Velocity Distribution

The energy dissipation efficiency of the BSDE was solved by the Bernoulli Eq. (14b). The results showed that the energy dissipation coefficient of the flow channel was 584–1701 at 5–15 m in the 25 experiment schemes (Table 5), which showed that the energy dissipation efficiency was obvious.

Taking scheme 1 (maximum energy dissipation coefficient) and scheme 25 (minimum energy dissipation coefficient) under 50 kpa pressure as the example. The fluid velocity at all points in the flow channel was not the absolute flow velocities in the BSDE (Fig. 7). However, the compared velocities within different locations in the flow channel were valid. By observing the velocity distribution of the two BSDE models, low-speed zone will be generated at the junction of the pit aperture, and high-speed zone will be generated at the left side of the tours. Experimental scheme 25 also produced obvious low-speed zones in the upper and lower corners. In the different low-speed zones of the BSDE model, a complete low-speed vortex was not observed, which had a good anti-blocking performance. The analysis of the flow velocity distribution and geometric parameters showed that the energy dissipation efficiency of the BSDE model was related to the flow rate and velocity distribution, the low-speed mixing of the junction area was conducive to energy dissipation.

Table 5: Energy dissipation coefficient of BSDE in different schemes at 5–15 m

Scheme	Energy dissipation coefficient	Scheme	Energy dissipation coefficient
1	1674~1701	14	847~872
2	1208~1235	15	811~838
3	975~995	16	937~953
4	786~803	17	1012~1089
5	643~655	18	1073~1161
6	1088~1113	19	761~805
7	852~860	20	597~605
8	1011~1087	21	999~1064
9	822~838	22	1074~1101
10	839~844	23	782~806
11	1167~1200	24	721~749
12	941~960	25	584~613
13	764~799		
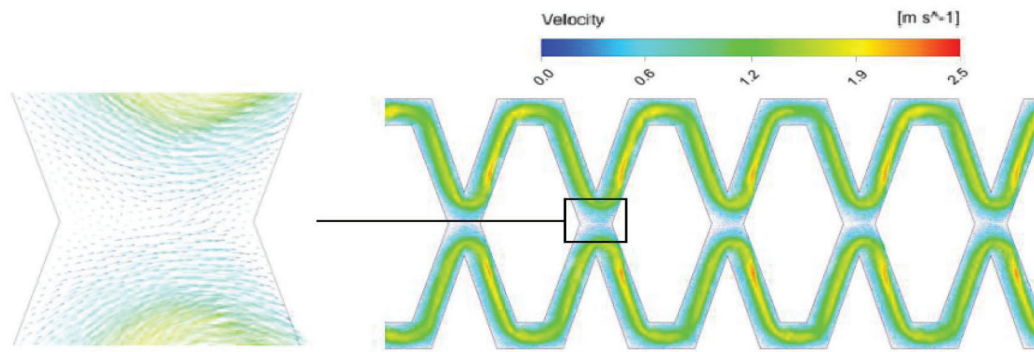
(a) Experimental scheme 1
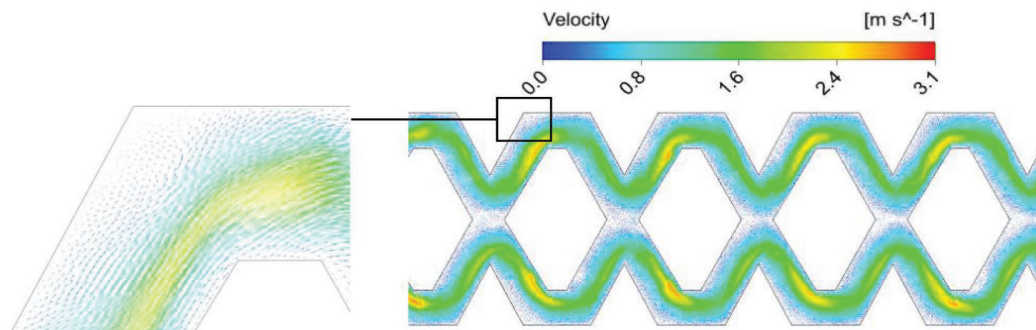
(b) Experimental scheme 25

Figure 7: Relationship between flow rate and pressure for experimental schemes 1 and 25

3.3 Influencing Factors of Flow Index

The range analysis of geometric parameters was implemented through the flow index values in Table 4. The range value showed that the order of the influence of each geometric parameter on the flow index was A > B > C > D > E. The optimal solution was A0.6B1.0C0.3D0.12E0.21 (Table 6).

Table 6: Range analysis results for orthogonal experiment

Scheme	Flow index					
	Level	A/mm	B/mm	C/mm	D/mm	E/mm
Ki value	1	2.4917	2.4818	2.4635	2.4813	2.4394
	2	2.4796	2.4691	2.4691	2.4774	2.4507
	3	2.4541	2.4245	2.4245	2.4553	2.4552
	4	2.4305	2.4506	2.4514	2.4414	2.4757
	5	2.4392	2.4691	2.4345	2.4397	2.4741
Ki avg value	1	0.4983	0.4964	0.4927	0.4963	0.4879
	2	0.4959	0.4938	0.4938	0.4955	0.4901
	3	0.4908	0.4849	0.4849	0.4911	0.4910
	4	0.4861	0.4901	0.4903	0.4883	0.4951
	5	0.4878	0.4938	0.4869	0.4880	0.4948
Best level		1	1	2	1	4
R		0.0122	0.0115	0.0089	0.0083	0.0073
Number of levels		5	5	5	5	5
Number of repeats per level r		5	5	5	5	5

Note: Ki is sum of flow index for level i; Ki avg is arithmetic mean of Ki.

Further analysis of the trend of the relationship between each parameter and the flow index (Fig. 8), it can be seen that the flow index decreased with the increase of A, B, C and D, and increased with the increase of E.

3.4 Establishment and Verification of Flow Index Prediction Model

Based on the results of the orthogonal experiment, SPSS software was used to perform a multiple linear regression with a confidence level of 95%, and the regression model between the flow index and each parameter was calculated as:

$$x = 0.5411 - 0.0308A - 0.0088B - 0.0319C - 0.0795D + 0.0629E \tag{17}$$

The regression coefficient significance test F statistic value of this model was 6.997, the significance level Sig.= 0.001, the regression effect was significant, and the established regression equation was effective.

In order to further verify the reliability of the regression model, three groups of different flow channels were selected within the range of geometric parameters (Table 7), and the model samples were processed for testing and simulation. The estimated value was calculated by the formula (17) and the relative error was calculated by the formula (16). The calculation showed that the relative error of the flow index was −1.03% to 0.74%, which was less than 3%, indicating that the regression model of the formula (17) can accurately reflect the quantitative relationship between the flow index and the geometric parameters of the BSDE.
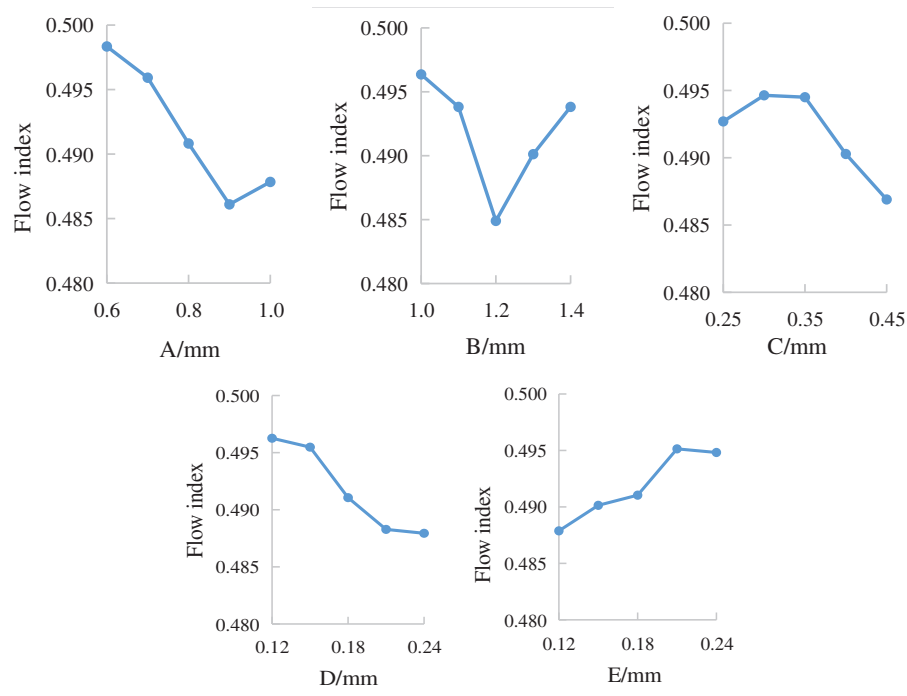
Figure 8: Effect of geometric parameter on flow index

Table 7: Verification scheme and results

Level	Geometry parameters values					Flow index			Error/%	
	A/mm	B/mm	C/mm	D/mm	E/mm	Simulation value	Test value	Estimated value	S-E	T-E
1	0.6	1.0	0.35	0.18	0.18	0.5025	0.4946	0.4997	0.56%	-1.03%
2	0.8	1.1	0.40	0.15	0.12	0.4890	0.4849	0.4896	-0.12%	-0.97%
3	0.9	1.3	0.40	0.21	0.15	0.4855	0.4810	0.4819	0.74%	-0.19%

4 Conclusion

1. The flow index of the BSDE was 0.4757–0.5067, indicating that its hydraulic performance was good. The energy dissipation coefficient under the pressure head of 5–15 m was 584–1701. Compared with the traditional unit flow channel structure, the energy loss effect was significantly improved, indicating that the structure of this type of drip irrigation emitter was reasonable.

2. There was no low-speed vortex zone in the model flow channel, and the low-speed mixing of the junction area was conducive to energy dissipation. The results showed that the flow index decreased with the increase of A, B, C and D, and increased with the increase of E. The influence order of the geometric parameters on the flow index was A > B > C > D > E, The optimal solution was $A_{0.6}B_{1.0}C_{0.3}D_{0.12}E_{0.21}$.

3. The flow index prediction model was established, and the relative error among the test value, simulated value and estimated value was less than 3%, which proved the accuracy and reliability of the regression model.

Conflicts of Interest: The authors declare that they have no conflicts of interest to report regarding the present study.

References

1. Madramootoo, C. A., Morrison, J. (2013). Advances and challenges with micro-irrigation. *Irrigation and Drainage, 62(3),* 255–261. DOI 10.1002/ird.1704.

2. Al-Amoud, A. I., Mattar, M. A., Ateia, M. I. (2014). Impact of water temperature and structural parameters on the hydraulic labyrinthchannel emitter performance. *Spanish Journal of Agricultural Research, 12(3),* 580–593. DOI 10.5424/sjar/2014123-4990.

3. Liu, C. J., Tang, D. B., Wang, L., Zhao, Z. (2016). Multi output optimization of the hydraulic performance for drip irrigation trapezoidal labyrinth channel of emitter. *Arid Land Geography, 39(3),* 600–606. DOI 10.13826/j.cnki.cn65-1103/x.2016.03.017.

4. Souza, W. D. J., Sinobas, L. R., Sánchez, R., Botrel, T. A., Coelho, R. D. (2014). Prototype emitter for use in subsurface drip irrigation: Manufacturing, hydraulic evaluation and experimental analyses. *Biosystems Engineering, 128(2),* 41–51. DOI 10.1016/j.biosystemseng.2014.09.011.

5. Ozekici, B., Sneed, R. E. (1991). *Analysis of pressure losses in tortuous-path emitters*, pp. 23–26. American Society of Agricultural Engineers (USA), Albuquerque, New Mexico. https://agris.fao.org/agris-search/search.do?recordID=US9511213.

6. Feng, J., Li, Y., Wang, W., Xue, S. (2018). Effect of optimization forms of flow path on emitter hydraulic and anti-clogging performance in drip irrigation system. *Irrigation Science, 36(1),* 37–47. DOI 10.1007/s00271-017-0561-9.

7. Mohamed, A. M., Ahmed, I. A. (2017). Gene expression programming approach for modeling the hydraulic performance of labyrinth-channel emitters. *Computers and Electronics in Agriculture, 142(2),* 450–460. DOI 10.1016/j.compag.2017.09.029.

8. Vekariya, P. B., Subbaiah, R., Mashru, H. H. (2011). Hydraulics of microtube emitters: A dimensional analysis approach. *Irrigation Science, 29(4),* 341–350. DOI 10.1007/s00271-010-0240-6.

9. Wang, H. X., Zhang, X. Y., Niu, W. Q., Liu, M., Li, B. (2020). The effect of temperature on emitter clogging in low-pressure drip fertilization system. *Journal of Irrigation and Drainage, 39(3),* 63–71. DOI 10.13522/j.cnki.ggps.2019157.

10. Hu, Y. X., Peng, J. Z., Yin, F., Liu, X. F., Li, N. (2020). Optimization and parameter analysis of trapezoidal labyrinth emitter channel based on MATLAB and COMSOL co-simulation. *Transactions of the Chinese Society of Agricultural Engineering, 36(22),* 158–164. DOI 10.11975/j.issn.1002-6819.2020.22.017.

11. Philipova, N., Nikolov, N., Pichurov, G., Markov, D. (2009). Numerical simulation and a mathematical model of pressure losses depending on geometric parameters of drip emitter labyrinth channel. *Comptes Rendus De l'Académie Bulgare Des Sciences: Sciences Mathématiques Et Naturelles, 62(7),* 891–898.

12. Demir, V., Yurdem, H. U., Yazgi, A., Gunhan, T. U. (2019). Measurement and prediction of total friction losses in drip irrigation laterals with cylindrical integrated in-line drip emitters using CFD analysis method. *Journal of Agricultural Sciences, 25(3),* 354–366. DOI 10.15832/ankutbd.433830.

13. Baghel, Y. K., Kumar, J., Patel, V. K. (2021). CFD Analysis of the flow characteristics of in-line drip emitter with different labyrinth channels. *Journal of the Institution of Engineers (India): Series A, 102(1),* 111–119. DOI 10.1007/s40030-020-00499-5.

14. Yuan, W. J., Wei, Z. Y., Chu, H. L., Ma, S. L. (2014). Optimal design and experiment for divided-flow emitter in drip irrigation. *Transactions of the Chinese Society of Agricultural Engineering, 30(17),* 117–124. DOI 10.3969/j.issn.1002-6819.2014.17.016.

15. Guo, L., Bai, D., Wang, X. D., He, J., Zhou, W. et al. (2016). Hydraulic performance and energy dissipation effect of two-ways mixed flow emitter in drip irrigation. *Transactions of the Chinese Society of Agricultural Engineering, 32(17),* 77–82. DOI 10.11975/j.issn.1002-6819.2016.17.011.

16. Wu, F., Dong, X. S., Wu, Y. B., Ma, D., Feng, X. F. (2017). Hydraulic properties of the flow in a gradual shrinking and sudden enlarging channel. *Journal of North China University of Water Resources and Electric Power, 38(2),* 61–67. DOI 10.3969/j.issn.1002-5634.2017.02.012.

17. Yurdem, H., Demir, V., Mancuhan, A. (2015). Development of a simplified model for predicting the optimum lengths of drip irrigation laterals with coextruded cylindrical in-line emitters. *Biosystems Engineering, 137(1),* 22–35. DOI 10.1016/j.biosystemseng.2015.06.010.

18. Li, Y., Yang, P., Ren, S. (2007). Effects of fractal flow part designing and its parameters on emitter hydraulic performance. *Chinese Journal of Mechanical Engineering, 43(7),* 109–114. DOI 10.3901/JME.2007.07.109.

19. Guo, L., Bai, D., Cheng, P., Zhou, W. (2015). Optimization design of triangular labyrinth channel in drip irrigation emitter. *Journal of Drainage and Irrigation Machinery Engineering, 33(7),* 634–639. DOI 10.3969/j.issn.1674-8530.14.0164.

20. Tian, J. Y., Bai, D., Ren, C. J., Wang, X. D. (2013). Analysis on hydraulic performance of bidirectional flow channel of drip irrigation emitter. *Transactions of the Chinese Society of Agricultural Engineering, 29(20),* 89–94. DOI 10.3969/j.issn.1002-6819.2013.20.013.

21. Xing, S., Wang, Z., Zhang, J., Liu, N. N., Zhou, B. (2021). Simulation and verification of hydraulic performance and energy dissipation mechanism of perforated drip irrigation emitters. *Water, 13(2),* 171. DOI 10.3390/w13020171.

22. Xu, T., Zhang, L. (2019). Hydraulic performance and energy dissipation effect of pit structure flow channel emitter. *IFAC-PapersOnLine, 52(30),* 143–148. DOI 10.1016/j.ifacol.2019.12.512.

23. Xu, T., Zhang, L. (2020). Influence and analysis of structure design and optimization of a pit drip irrigation emitter on the performance. *Irrigation and Drainage, 69(4),* 633–645. DOI 10.1002/ird.2433.

24. Ryad, C., Djamel, S., Adel, S., Smail, M. (2019). Numerical simulation of double diffusive mixed convection in a horizontal annulus with fifinned inner cylinder. *Fluid Dynamics & Materials Processing, 15(2),* 153–169. DOI 10.32604/fdmp.2019.04294.

25. Basri, A. A., Zuber, M., Basri, E. I., Zakaria, M. S., Aziz, A. F. A. et al. (2021). Fluid-structure interaction in problems of patient specific transcatheter aortic valve implantation with and without paravalvular leakage complication. *Fluid Dynamics & Materials Processing, 17(3),* 531–553. DOI 10.32604/fdmp.2021.010925.